SPECTRAL MODEL FOR WAVE TRANSFORMATION AND BREAKING OVER IRREGULAR BATHYMETRY

By Arun Chawla,[1] H. Tuba Özkan-Haller,[2] and James T. Kirby[3]

ABSTRACT: A numerical model is presented that predicts the evolution of a directional spectral sea state over a varying bathymetry using superposition of results of a parabolic monochromatic wave model run for each initial frequency-direction component. The model predicts dissipation due to wave breaking using a statistical breaking model and has been tested with existing data for unidirectional random waves breaking over a plane beach. Experiments were also conducted for a series of random directional waves breaking over a circular shoal to test the model in a two-dimensional wave field. The model performs well in both cases, although directional effects are not included in the breaking dissipation formulation.

INTRODUCTION

The modeling of ocean wave propagation over a varying bathymetry is a subject of considerable interest to coastal engineers, and has advanced a great deal in the last two decades since the development of the classical mild slope equation by Berkhoff (1972). A number of approximations have been made to the mild slope equation to increase the efficiency of model prediction. One such approximation, which has gained popularity primarily because of the speed of computation, is the parabolic approximation, used in water waves for the first time by Radder (1979). The parabolic model equation is based on the assumption that waves propagate within a limited range of angles about an assumed propagation direction. Nonlinear formulations of parabolic equations (Kirby and Dalrymple 1983) have been found to give more accurate results than the linear mild slope equation for the case of monochromatic waves transforming over a submerged shoal (Kirby and Dalrymple 1984). Although these models are limited by the range of angles over which accurate results can be obtained, this limitation can be relaxed using either techniques to increase the range of allowed angles [e.g., Padé approximants (Booij 1981) and minimax approximations (Kirby 1986b)], or curvilinear coordinate systems (Isobe 1987) to have the grid correspond more closely to the wave propagation direction. In addition, the models can be enhanced to include the effects of strong currents (Kirby 1986a).

Although relatively accurate parabolic models have been developed to study the evolution of waves over an irregular bottom, all these models have been derived for monochromatic waves only. Coastal engineers have traditionally approximated the irregular sea state offshore using a representative monochromatic wave in order to use these models for predictions. However, investigators such as Goda (1985) (using an analytical approach), Vincent and Briggs (1989) (by conducting an experimental study), and Panchang et al. (1990) (using a numerical approach) have shown that such an approximation may result in large errors due to vast dissimilarities in the refraction-diffraction patterns resulting from monochromatic and irregular wave fields.

Recently, methods for computing the evolution characteristics of a directional spectral sea state using monochromatic wave models have been developed. A good theoretical background can be obtained from Izumiya and Horikawa (1987). Panchang et al. (1990) and Grassa (1990) have each developed models using a spectral calculation method based on the discretization of the offshore spectrum into individual monochromatic directional components. The transformation of each component can then be determined with the help of a monochromatic parabolic model. The statistical characteristics of the spectrum at the grid points are obtained by assembling the wave components by linear superposition. O'Reilly and Guza (1991) have further extended this formulation and have pointed out that the model could be used (in linear form) to develop a transfer function between offshore and onshore, after which any incident spectrum could be simply transformed using the computed transfer function.

Due to significant variations in bathymetry and ambient current fields in the nearshore region, the wave field experiences strong modifications that lead to depth-limited and current-limited breaking, causing significant energy losses in the wave field. This effect is not included in the models described previously. The purpose of this study is to alleviate these restrictions and provide a platform for predicting strong breaking energy losses in a directional spectral sea. In this paper, we are limiting ourselves to parabolic spectral modeling of swell waves.

In this study, a numerical model (REF/DIF S) has been developed that uses the parabolic refraction-diffraction formulation of Kirby (1986a) to model the evolution of directional random waves in the nearshore region. A statistical energy dissipation model by Thornton and Guza (1983) is incorporated to predict realistically energy losses due to wave breaking. The model is tested on an existing experimental data set of Mase and Kirby (1992), which considers depth-limited breaking during the propagation of a unidirectional random wave field on a plane beach. To study the accuracy of the model in a two-dimensional wave field, experimental studies of irregular waves transforming and breaking over a circular shoal were conducted. The experiments were carried out for two different directional spreadings and total energies. Data-to-model comparisons are used to determine how well the model estimates the wave field for a range of breaking wave conditions. It is worth mentioning that O'Reilly and Guza (1991) showed that, in the case of very broad directional spreading, diffraction effects become unimportant, and a wave refraction model can be used just as accurately. In such situations, perhaps a simpler spectral refraction model with a sink term to account for wave breaking would be preferable to the more complex refraction-diffraction model.

[1]Grad. Student, Ctr. for Appl. Coast. Res., Dept. of Civ. and Envir. Engrg., Univ. of Delaware, Newark, DE 19716.

[2]Postdoct. Fellow, Ctr. for Appl. Coast. Res., Dept. of Civ. and Envir. Engrg., Univ. of Delaware, Newark, DE; and Ocean and Coast. Res. Group, Univ. of Cantabria.

[3]Prof., Ctr. for Appl. Coast. Res., Dept. of Civ. and Envir. Engrg., Univ. of Delaware, Newark, DE.

Note. Discussion open until January 1, 1999. To extend the closing date one month, a written request must be filed with the ASCE Manager of Journals. The manuscript for this paper was submitted for review and possible publication on June 17, 1996. This paper is part of the ***Journal of Waterway, Port, Coastal, and Ocean Engineering***, Vol. 124, No. 4, July/August, 1998. ©ASCE, ISSN 0733-950X/98/0004-0189–0198/ $8.00 + $.50 per page. Paper No. 13416.

DESCRIPTION OF MODELING SCHEME

The parabolic model for spectral wave conditions used here simulates the evolution of directional random waves in the nearshore zone. The model predicts the effects of refraction, diffraction, shoaling, and breaking. It is particularly applicable to regions where an incoming random sea propagates over a complicated bathymetry towards the shore. The bathymetry may include a shoal formation at the mouth of an inlet or estuary, where refraction, diffraction, shoaling, and depth-limited breaking will simultaneously be important.

The model requires the input of the incoming directional random sea at the offshore boundary. The random sea is represented by a two-dimensional spectrum which is discretized (in frequency and direction) into wave components. Given values for the wave amplitudes of the components at the offshore boundary, the parabolic approximation enables us to obtain solutions by marching in the assumed propagation direction. Using this forward-stepping algorithm, the evolution of the amplitudes of all wave components can be computed simultaneously. Therefore, after each forward step it is possible to determine statistical quantities at that row before taking another step forward. These quantities are incorporated into a statistical wave breaking model.

Wave Model for Individual Wave Components

It is assumed that the water surface elevation η is periodic in time and that the spatial dependency can be split into a fast-varying phase and a slow-varying amplitude. Indices j and l shall be used to represent frequency and direction, respectively. Choosing a coordinate system such that the x-axis points in the propagation direction, the water surface elevation can be represented by

$$\eta = \sum_j \sum_l \eta_{jl} = \text{Re}\left\{\sum_{j=1}^{N_f} \sum_{l=1}^{N_\theta} A_{jl}(x, y) e^{[i(\bar{k}_j x - \omega_j t)]}\right\} \tag{1}$$

where Re(Z) denotes the real part of a complex number Z; and $A_{jl}(x, y)$ = the slowly varying complex wave amplitude for a wave component jth in frequency and lth in direction. N_f and N_θ = number of discretizations in frequency and direction, respectively. Also, $k_j(x, y)$ = wave number; and ω_j = angular frequency at the jth frequency component, related by

$$\omega_j^2 = g k_j \tanh k_j h$$

A representative value of the wavenumber at the jth frequency is defined according to

$$\bar{k}_j(x) = \frac{1}{B} \int_0^B k_j(x, y)\, dy$$

where B = width of the domain. It should be noted that if the wave field consists of only plane waves, then $A_{jl}(x, y)$ can be written in terms of a constant amplitude and direction as

$$A_{jl} = a_{jl} e^{[i(k_j \cos\theta_{jl} - \bar{k}_j)x + i k_j \sin\theta_{jl} y]} \tag{2}$$

The refraction, diffraction, and shoaling of discrete wave components is assumed to be governed by the parabolic approximation to a wave-current mild slope equation derived by Kirby (1984). To minimize the restrictions placed on the range of allowed wave angles with respect to the assumed wave direction, the procedure derived by Booij (1981) is used, enabling the model to handle wave directions up to about ±45° from the x direction. The governing equation in the model for the complex wave amplitude $A_{jl}(x, y)$ is given by (Kirby 1986a)

$$\begin{aligned}
&(C_{gj} + U)(A_{jl})_x - 2\Delta_1 V(A_{jl})_y + i(\bar{k}_j - a_0 k_j)(C_{gj} + U)A_{jl} \\
&+ \left\{\frac{\sigma_j}{2}\left(\frac{C_{gj} + U}{\sigma_j}\right)_x - \Delta_1 \sigma_j \left(\frac{V}{\sigma_j}\right)_y\right\} A_{jl} \\
&+ i\Delta_j' \left[((CC_g)_j - V^2)\left(\frac{A_{jl}}{\sigma_j}\right)_y\right]_y \\
&- i\Delta_1 \left\{\left[UV\left(\frac{A_{jl}}{\sigma_j}\right)_y\right]_x + \left[UV\left(\frac{A_{jl}}{\sigma_j}\right)_x\right]_y\right\} + \alpha A_{jl} \\
&+ \frac{-b_1}{k_j}\left\{\left[((CC_g)_j - V^2)\left(\frac{A_{jl}}{\sigma_j}\right)_y\right]_{yx} + 2i\left(\sigma_j V\left(\frac{A_{jl}}{\sigma_j}\right)_y\right)_x\right\} \\
&+ b_1\beta_j\left\{2i\omega_j U\left(\frac{A_{jl}}{\sigma_j}\right)_x + 2i\sigma_j V\left(\frac{A_{jl}}{\sigma_j}\right)_y - 2UV\left(\frac{A_{jl}}{\sigma_j}\right)_{xy}\right. \\
&\left. + \left[((CC_g)_j - V^2)\left(\frac{A_{jl}}{\sigma_j}\right)_y\right]_y\right\} - \frac{i}{k_j} b_1\{(\omega_j V)_y + 3(\omega_j U)_x\}\left(\frac{A_{jl}}{\sigma_j}\right)_x \\
&- \Delta_2\left\{\omega_j U\left(\frac{A_{jl}}{\sigma_j}\right)_x + \frac{1}{2}\omega_j U_x\left(\frac{A_{jl}}{\sigma_j}\right)\right\} + i k_j \omega_j U(a_0 - 1)\left(\frac{A_{jl}}{\sigma_j}\right) = 0
\end{aligned} \tag{3}$$

where $U(x, y)$ and $V(x, y)$ = currents in the x and y directions, respectively; $C_{gj}(x, y)$ = group velocity; and $C_j(x, y)$ = phase velocity at the jth frequency. Also,

$$\sigma_j = \omega_j - k_j U; \quad \beta_j = \frac{(k_j)_x}{k_j^2} + \frac{(k_j((CC_g)_j - U^2))_x}{2k_j^2((CC_g)_j - U^2)} \tag{4a,b}$$

$$\Delta_1 = a_1 - b_1; \quad \Delta_2 = 1 + 2a_1 - 2b_1; \quad \Delta_j' = a_1 - b_1\frac{\bar{k}_j}{k_j} \tag{4c–e}$$

The model coefficients

$$a_0 = 1; \quad a_1 = -0.75; \quad b_1 = -0.25 \tag{5a–c}$$

recover the Padé approximant of Booij (1981).

Given the complex amplitudes for the wave components at the offshore row, the evolution of all wave components as they travel towards shore can be computed simultaneously at each row, and the spectrum can be evaluated at any grid point by a superposition of the different wave components as shown in the following section.

An estimate for the wave angle at each model grid point can be obtained using the computed complex amplitude A_{jl}. These estimates are then used in calculating the radiation stress terms and constructing the directional spectrum. Assuming a plane wave construction for the surface elevation and using (2), we can obtain the wave angle at each grid point as

$$\theta_{jl} = \arctan\left[\frac{\dfrac{\partial \text{Im}(\ln A_{jl})}{\partial y}}{\dfrac{\partial \text{Im}(\ln A_{jl})}{\partial x} + \bar{k}_j}\right] \tag{6}$$

where Im(Z) denotes the imaginary part of a complex number Z.

A drawback to using this method to determine the wave angle is that it fails at the nodal points of a short-crested wave pattern. These patterns are commonly generated due to wave focusing over irregular bathymetry such as submerged shoals. However, the resulting irregular angles occur at points where the component wave amplitudes are low; hence they have minimal impact on the estimate of radiation stresses or corresponding mean angles, whose calculation is described later in the paper.

Wave Climate

The discretization process of the two-dimensional spectrum results in wave components of amplitude A_{jl} with an associated frequency f_j and an angle of incidence θ_l. To determine energy losses associated with randomly occurring wave breaking (see the following section), it is necessary to have estimates of the statistical wave height at each point in the model grid as the computation passes that point. Assuming a Rayleigh distribution of the wave heights and using the computed information about the spectral components at a location (x, y), the significant wave height can be computed as

$$H_s(x, y) = \left(8 \sum_{j=1}^{N_f} \sum_{l=1}^{N_\theta} |A_{jl}(x, y)|^2 \right)^{1/2} \tag{7}$$

Other statistical quantities such as the frequency spectrum $S(f)$, the directional spectrum $S(f, \theta)$, and the average angle $\bar{\theta}$ can also be obtained. The frequency spectrum is obtained by summing up the energy of all the wave components with the same frequency. Energy is then obtained as a function of the frequency, and the spectrum is obtained by scaling the energy with the corresponding bin widths for the frequencies. The frequency spectrum is thus given by

$$S(f_j) = \frac{\sum_{l=1}^{N_\theta} |A_{jl}(x, y)|^2}{2(\delta f_j)} \tag{8}$$

where $j = 1, \ldots, N_f$; and δf_j = bin width for frequency f_j.

Instead of determining the energy for each frequency and angle, estimates of the directional spectrum are made by dividing the angular range from $\theta = -92.5°$ to $\theta = 92.5°$ into 37 bins with a bin width of 5°. For each frequency, the wave components are sorted into the different bins based on their directions obtained from (6). The energy is then summed for each bin, and again scaled by the frequency bin width and the angle bin width to obtain the energy density. The representative angle of each angular bin is taken as the mean angle of that bin (e.g., the angle for the bin $\theta = 42.5°$ to $\theta = 47.5°$ is given by $\theta = 45°$). The directional spectrum is thus given by

$$S(f_j, \theta_b) = \frac{\sum_{l=\mathcal{L}_{jb}^{(1)}}^{\mathcal{L}_{jb}^{(2)}} |A_{jl}(x, y)|^2}{2\delta f_j \delta\theta} \tag{9}$$

where $b = 1, \ldots, 37$; $\mathcal{L}_{jb}^{(1)}$ to $\mathcal{L}_{jb}^{(2)}$ = wave components at the jth frequency that lie in the bth directional bin; and θ_b = representative angle of the bin.

An average angle estimate at each grid point is also made to determine the mean angle of the spectrum, with the help of radiation stress estimates. Radiation stress for a monochromatic wave is defined here as the depth-integrated wave-averaged stress due to the wave. The expressions for the radiation stress terms for each wave component moving at an angle θ to the x axis are determined using linear theory. The total radiation stress at any point in the field then is the sum of all radiation stress contributions at that point, and is given by

$$S_{xx} = \frac{1}{2} \sum_{j=1}^{N_f} \sum_{l=1}^{N_\theta} |A_{jl}|^2 \left[n_j(1 + \cos^2\theta_{jl}) - \frac{1}{2} \right] \tag{10a}$$

$$S_{yy} = \frac{1}{2} \sum_{j=1}^{N_f} \sum_{l=1}^{N_\theta} |A_{jl}|^2 \left[n_j(1 + \sin^2\theta_{jl}) - \frac{1}{2} \right] \tag{10b}$$

$$S_{xy} = \frac{1}{4} \sum_{j=1}^{N_f} \sum_{l=1}^{N_\theta} |A_{jl}|^2 n_j \sin(2\theta_{jl}) \tag{10c}$$

where S_{xx} = radiation stress acting on the x plane along the x direction; S_{yy} = radiation stress acting on the y plane along the y direction; S_{xy} = radiation stress acting on the y plane along the x direction (due to symmetry of the stress tensor $S_{yx} = S_{xy}$); and n_j = ratio of the group velocity C_{gj} to the phase velocity C_j. It is given in terms of wave number k_j and water depth h by

$$n_j = \frac{1}{2} \left(1 + \frac{2k_j h}{\sinh(2k_j h)} \right)$$

The radiation stress terms defined in (10) are scaled by a constant factor ρg, where ρ = density of water and g = acceleration due to gravity.

The average angle at any particular point in the field is defined as the angle that represents the total radiation stress at that point for the peak frequency and significant wave height at the same point. Thus, the angle is given by

$$\bar{\theta} = \frac{1}{2} \arcsin \left(\frac{32 S_{xy}}{(n_p H_s^2)} \right) \tag{11}$$

where n_p = ratio of the group velocity to the phase velocity for the peak frequency. It was pointed out in the previous section that over an irregular bathymetry where standing waves are formed, (6) gives incorrect results at the nodal points. This, however, does not affect the estimate of the average angle $\bar{\theta}$, because the individual angle estimates are weighted by their energy, which is small when angle estimates are inaccurate.

Breaking Model

The statistical information obtained after each step in the parabolic scheme is used to construct a model for the dissipation of energy due to breaking. The amount of energy dissipated is a function of the local statistical quantities and the local water depth. Therefore, breaking of individual waves in a wave train is not considered, but a spectral approach to the wave breaking process is taken.

Consider a linear shoaling model for a wave component at the jth frequency and the lth direction given by

$$C_{gj} \frac{\partial A_{jl}}{\partial x} + \frac{1}{2} \frac{\partial C_{gj}}{\partial x} A_{jl} = 0 \tag{12}$$

Adding a damping term to simulate wave breaking gives an evolution equation of

$$C_{gj} \frac{\partial A_{jl}}{\partial x} + \frac{1}{2} \frac{C_{gj}}{\partial x} A_{jl} = -\alpha A_{jl} \tag{13}$$

and a corresponding energy equation of

$$\frac{\partial (C_{gj} |A_{jl}|^2)}{\partial x} = -2\alpha |A_{jl}|^2 \tag{14}$$

Summing along frequency and direction, we get

$$\frac{\partial \left(\sum_{j=1}^{N_f} C_{gj} \sum_{l=1}^{N_\theta} |A_{jl}|^2 \right)}{\partial x} = -2\alpha \sum_{j=1}^{N_f} \sum_{l=1}^{N_\theta} |A_{jl}|^2 \tag{15}$$

Defining the root-mean-squared (rms) wave height

$$H_{rms}^2 = 4 \sum_{j=1}^{N_f} \sum_{l=1}^{N_\theta} |A_{jl}|^2$$

and substituting in (15) gives

$$\frac{\partial \left(\sum_{j=1}^{N_f} C_{gj} \sum_{l=1}^{N_\theta} |A_{jl}|^2 \right)}{\partial x} = -\frac{1}{2} \alpha H_{rms}^2 \tag{16}$$

A simple model by Thornton and Guza (1983) is used to determine the energy dissipation coefficient α. They express the energy dissipation as

$$\frac{\partial EC_g}{\partial x} = -\varepsilon_b \tag{17}$$

where the energy flux EC_g and the turbulent bore dissipation ε_b can be expressed as

$$EC_g = \frac{1}{2}\rho g \sum_{j=1}^{N_f} C_{gj} \sum_{l=1}^{N_\theta} |A_{jl}|^2 \tag{18}$$

and

$$\varepsilon_b = \frac{3\sqrt{\pi}}{16}\frac{\rho g \bar{f} B^3}{\gamma^4 h^5} H_{rms}^7 \tag{19}$$

Here, h = local water depth; and $\bar{f}$ = a representative frequency for the frequency spectrum that is chosen to be the peak frequency. Following Mase and Kirby (1992), the constants B and γ are chosen to be equal to 1 and 0.6, respectively.

Substituting for EC_g and ε_b in (17) and simplifying gives

$$\alpha = \frac{3\sqrt{\pi}}{4}\frac{\bar{f} B^3}{\gamma^4 h^5} H_{rms}^5 \tag{20}$$

Thus, an energy dissipation model can be built into the evolution equation by the addition of a wave breaking term αA_{jl}, where α is given by (20). The magnitude of the coefficient α is infinitesimally small when breaking does not occur but grows to a significant value when breaking starts to occur. Furthermore, the presence of the breaking term in the equation at all times makes any criterion for turning breaking on or off unnecessary. The dissipation coefficient has been assumed to be constant over the frequency domain. This leads to erroneous results when transfer of energy via wave-wave interactions takes place in the spectrum, and ideally, a dissipation coefficient with a strong dependence on frequency should be chosen (Kirby and Kaihatu 1996). As this is a linear model which does not simulate these interactions, a constant dissipation coefficient is appropriate.

The dissipation model of Thornton and Guza (1983) was originally derived assuming that the waves continue breaking once they have started to break. This would be the case for waves shoaling and breaking on a monotonic beach profile. In situations where an increase of the water depth is encountered after the waves start breaking, they will stop breaking and reform. This is exemplified by waves on a barred beach or over a shoal. The dissipation model used here was not derived for such instances and no modifications have been made to account for the possibility that the breaking waves reform. However, in practice, an increase in the water depth will cause the dissipation coefficient α to decrease, as it is inversely proportional to h^5. Also, no modifications have been made to Thornton and Guza's (1983) dissipation model to account for directional effects. Only the change in the energy flux in the x direction is considered.

DATA COMPARISONS FOR UNIDIRECTIONAL RANDOM WAVES

The model is tested for unidirectional random wave propagation on a plane beach using data by Mase and Kirby (1992). Qualitative comparisons with experimental data by Lie and Tørum (1991) showing the propagation of a unidirectional random wave field over a two-dimensional feature in the bathymetry were previously performed by Özkan (1993) with satisfactory results and will not be shown here.

Mase and Kirby (1992) conducted experiments using a Pierson-Moskowitz spectrum without directional spreading. The waves were generated in constant depth of 47 cm, and then shoaled and dissipated on a 1:20 beach. Wave gauges were placed at several locations on the beach. Fig. 1 shows the setup of the experiment in a wave flume.

Comparisons between this data set and the model will be made using Case 1 in Mase and Kirby (1992). The available data are in terms of time series of surface elevations at the wave gauge locations. The time series are used to compute the significant wave height for comparison with model results. Measured data at the offshore gauge is used to create a smoothed incident frequency spectrum for the model input. The incident spectrum is divided into 50 discrete wave components. Fig. 2 shows the incident frequency spectrum.

Results for wave heights in this case are presented in Fig. 3. It can be seen that the model predicts the shoaling and subsequent decay due to wave breaking reasonably well. The data points close to the shore show the presence of setup, which the model does not predict.

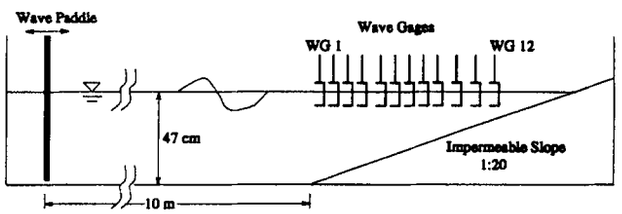

FIG. 1. Experimental Setup [from Mase and Kirby (1992)]

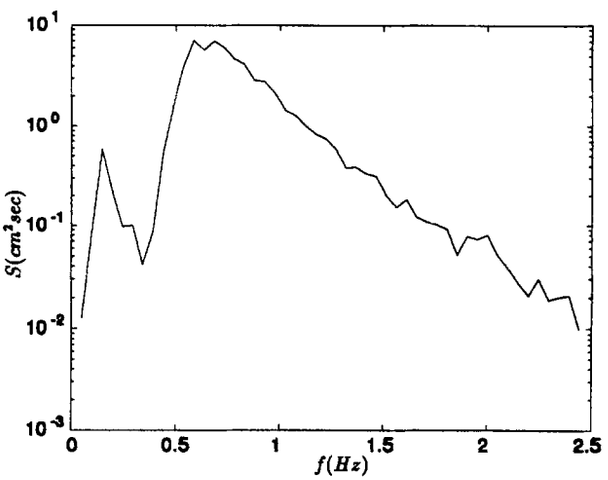

FIG. 2. Incident Frequency Spectrum

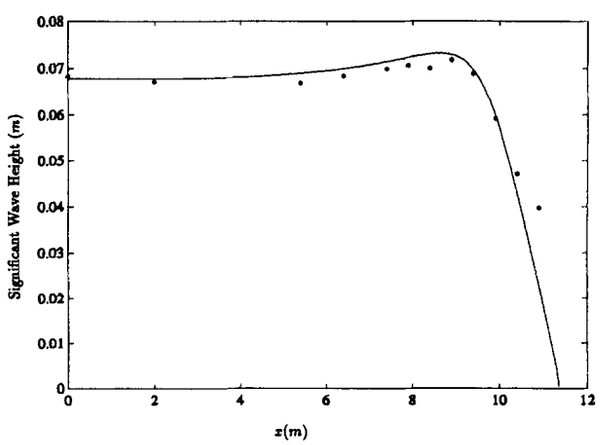

FIG. 3. Waves Shoaling on Beach: Significant Wave Height for Data and Model [$x(m)$ = Distance from Offshore Gauge in Meters]

DATA COMPARISONS FOR DIRECTIONAL RANDOM WAVES

Model comparisons with experimental data by Vincent and Briggs (1989) for directional random wave propagation over a submerged shoal were shown in an earlier study by Özkan and Kirby (1993). The comparisons for cases involving nonbreaking waves were very good, whereas the comparisons for cases that involved strong breaking on the shoal were characterized as inconclusive. To check predictions by the model and shed light on the processes involved during the propagation, shoaling, and breaking of a two-dimensional wave spectrum over a two-dimensional bathymetry, the need for a more comprehensive data set for various breaking wave conditions became apparent. Therefore, experiments were carried out in the directional wave basin at the University of Delaware. The following sections describe the experimental setup, data analysis, and model comparisons. For more detailed information, the reader is referred to Chawla (1995).

Experimental Setup

The wave basin is approximately 18 m long and 18.2 m wide. It has a three-dimensional wavemaker at one end consisting of 34 flap type paddles. The bottom is flat except for a circular shoal in the center and a stone beach at the far end to minimize reflections. A schematic view of the experimental layout together with the gauge locations is given in Fig. 4.

A total of ten capacitance gauges were used in the experiment, of which nine were placed in an array mounted on a movable frame. This array was then placed at fourteen different positions (denoted by thick lines in Fig. 4) to obtain a total of 126 measuring points around the shoal. Depending upon their orientation, one or more array positions form a transect along which comparisons are made with the numerical model. There is one longitudinal transect (A-A) going over the shoal and six transverse transects (B-B, C-C, D-D, E-E, F-F, and G-G) behind and on top of the shoal (see Fig. 4).

The center of the shoal is placed at $x = 5$ m and $y = 8.98$ m. The equation for the perimeter of the shoal is given by

$$(x - 5)^2 + (y - 8.98)^2 = (2.57)^2 \tag{21}$$

and for the bathymetry is given by

$$z = -(h + 8.73) + \sqrt{82.81 - (x - 5)^2 - (y - 8.98)^2} \tag{22}$$

where h = water depth away from the shoal.

The spectral sea state was obtained by using a TMA spectrum (Bouws et al. 1985) given by

$$E(f, h) = E_p(f)\phi_{pm}(f/f_p)\phi_j(f, f_p, \gamma, \sigma)\Phi_k(\omega_h) \tag{23}$$

with

$$E_p = \alpha g^2(2\pi)^{-4}f^{-5} \tag{24}$$

$$\phi_{pm} = \exp[-5/4(f/f_p)^{-4}]$$

$$\phi_j(f, f_p, \gamma, \sigma) = \exp[\ln(\gamma)\exp(-(f - f_p)^2/2\sigma^2 f_p^2)]$$

$$\sigma = \begin{cases} 0.07 & f \le f_p \\ 0.09 & f \ge f_p \end{cases}$$

$$\Phi_k(\omega_h) = \begin{cases} 0.5\omega_h^2 & \omega_h \le 1 \\ 1.0 & \omega_h \ge 2 \\ 1 - 0.5(2 - \omega_h)^2 & 1 < \omega_h < 2 \end{cases}$$

where f_p = peak frequency; ω_h = angular frequency normalized by the water depth h and is given by

$$\omega_h = 2\pi f\left(\frac{h}{g}\right)^{1/2}$$

α = a linear constant that can be scaled to obtain the desired variance; and γ = a factor which determines how broad the spectrum is (for our experiments we have taken $\gamma = 10$).

The directional distribution was modeled using a wrapped normal directional spreading function (Borgman 1984), given by

$$D(\theta) = \frac{1}{2\pi} + \frac{1}{\pi}\sum_{j=1}^{J}\left\{\exp\left[-\frac{(j\sigma_m)^2}{2}\right]\cos j(\theta - \theta_m)\right\} \tag{25}$$

where θ_m = mean wave direction; J = number of terms in the series (chosen as 50); and σ_m = a parameter which determines the width of the directional spreading.

Four different test conditions (Table 1) were run with h = 40 cm. The water depth on top of the shoal was 3 cm. All four tests had similar frequency spectra except that the energies in Tests 3 and 4 were lower (see Fig. 5). In all four cases, the waves were breaking on top of the shoal, with more waves breaking for Tests 5 and 6. Two different directional spread-

TABLE 1. Test Particulars for Spectral Tests

Test number (1)	H_{0s} (m) (2)	T_p (sec) (3)	θ_m (4)	σ_m (5)
3	0.0139	0.73	0	5
4	0.0156	0.73	0	20
5	0.0233	0.73	0	5
6	0.0249	0.71	0	20

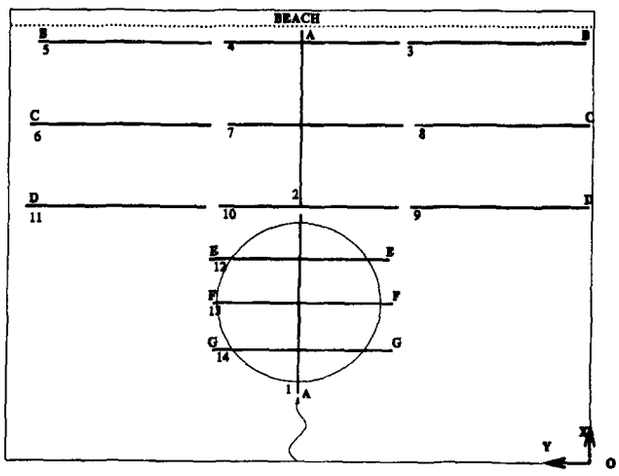

FIG. 4. Schematic View of Gauge Transect Locations and Experimental Setup

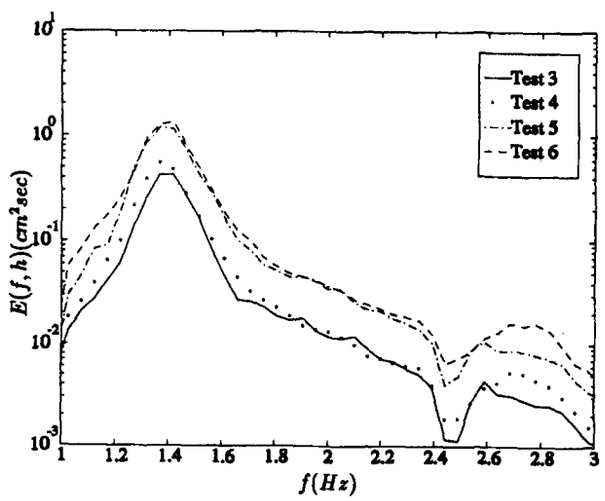

FIG. 5. Incident Frequency Spectra for Random Wave Tests

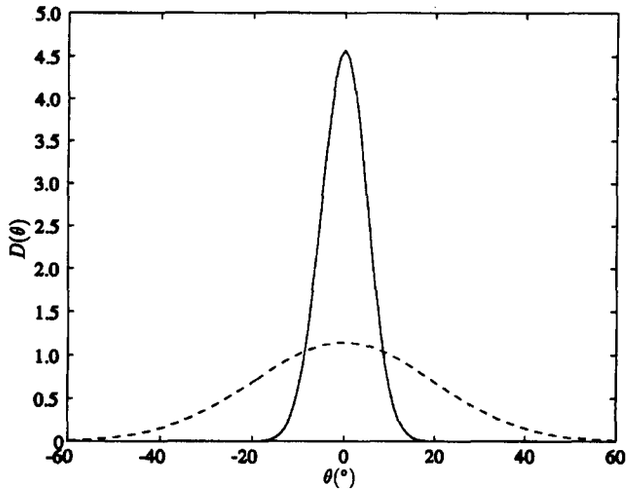

FIG. 6. Directional Distribution Used for Random Wave Tests

ings were used (Fig. 6), with the mean angle normal to the wavemaker ($\theta_m = 0°$). Tests 3 and 5 have a narrow directional spread, whereas Tests 4 and 6 have a broad directional spread. The initial significant wave height, H_{0s}, and the directional spreading parameter, σ_m, for the different test cases are given in Table 1. Data was collected at a sampling rate of 50 Hz for 32,768 sample points (≈900 waves) at all gauges.

Data Analysis and Comparison

The model was run using the initial significant wave heights given in Table 1. The incident spectrum was discretized into 30 components in frequency as well as 30 components in direction. Data to model comparisons were made for the significant wave heights and frequency spectra. Because the wave field is inhomogeneous due to refraction-diffraction effects, no estimates of the angular distribution were attempted using the data.

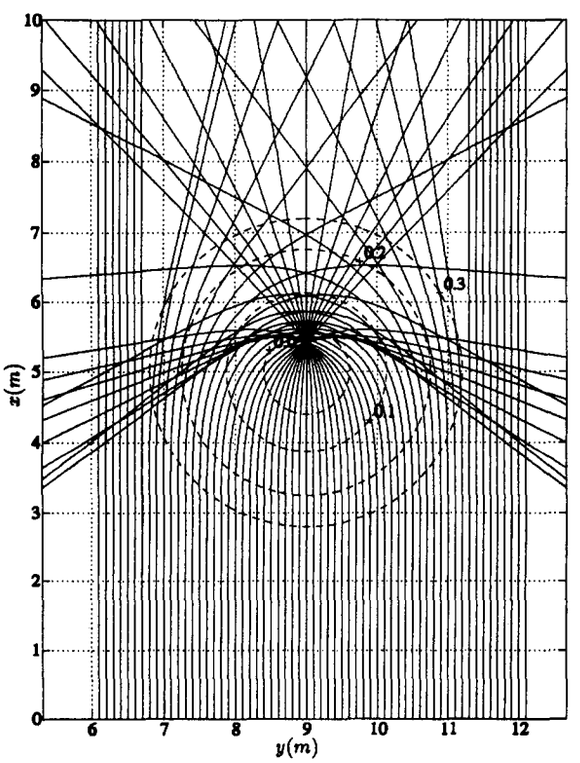

FIG. 7. Refraction Diagram at Peak Frequency f_p = 1.37 Hz for Given Bathymetry

Refraction patterns for the given bathymetry may be illustrated using ray theory techniques. A refraction pattern for a wave at the peak frequency is shown in Fig. 7. The focusing is quite severe, and on top of the shoal the wave rays can be moving at angles greater than 90°. Because the model can predict wave heights only within a range of ±45°, some discrepancies between model and data results are expected in this region.

Spatial Variation of Wave Height

The significant wave heights for the data and the model have been obtained from estimates of the variance, assuming a Rayleigh wave height distribution. A plot of the wave height distribution shows that this assumption is valid (Fig. 8). Reflections from the beach at the far end of the basin (see Fig. 4) are a matter of concern but have been ignored here because the reflected wave field could not be separated from the incident wave field. All the significant wave heights have been normalized with the input significant wave height H_{0s} to the model for the respective tests.

Figs. 9–12 give the wave height comparisons along transect A-A for the four different tests. The circles represent the data, whereas the solid line describes model predictions. The results are quite good except near the region of focus, where the

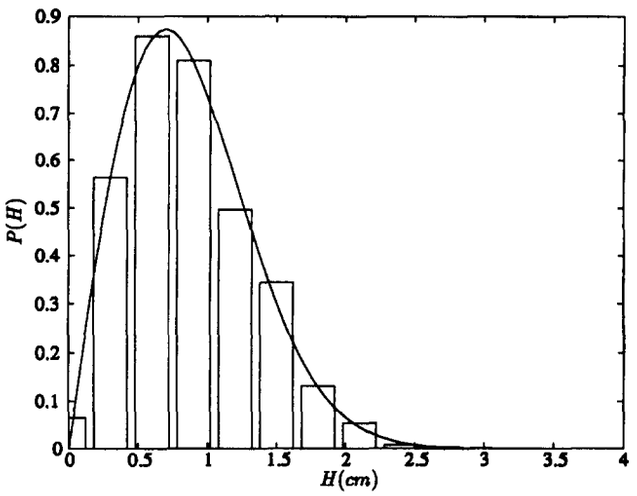

FIG. 8. Comparison of Rayleigh Distribution (Solid Line) to Weighted Wave Height Distribution (Bar Chart) in Front of Shoal for Test 3

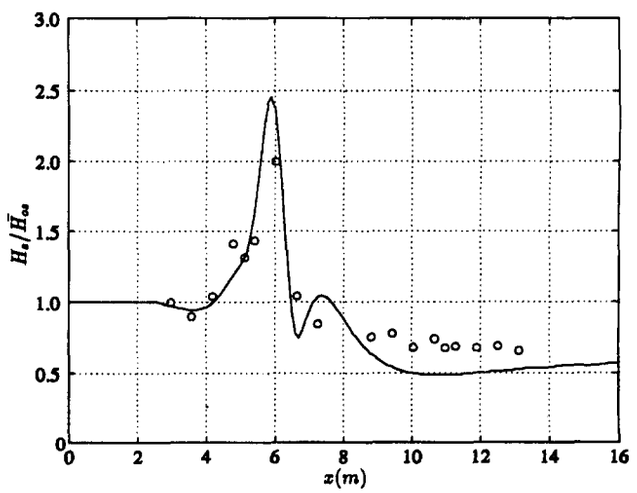

FIG. 9. Data-to-Model Comparisons of Significant Wave Heights along Transect A-A (Test 3: Less Energy, Narrow Directional Spread)

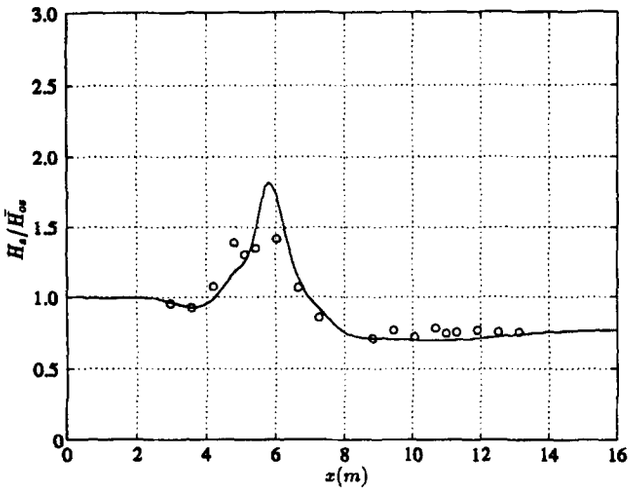

FIG. 10. Data-to-Model Comparisons of Significant Wave Heights along Transect A-A (Test 4: Less Energy, Broad Directional Spread)

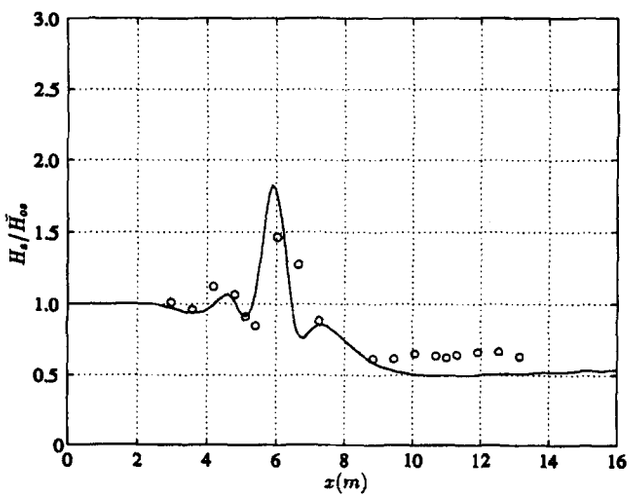

FIG. 11. Data-to-Model Comparisons of Significant Wave Heights along Transect A-A (Test 5: More Energy, Narrow Directional Spread)

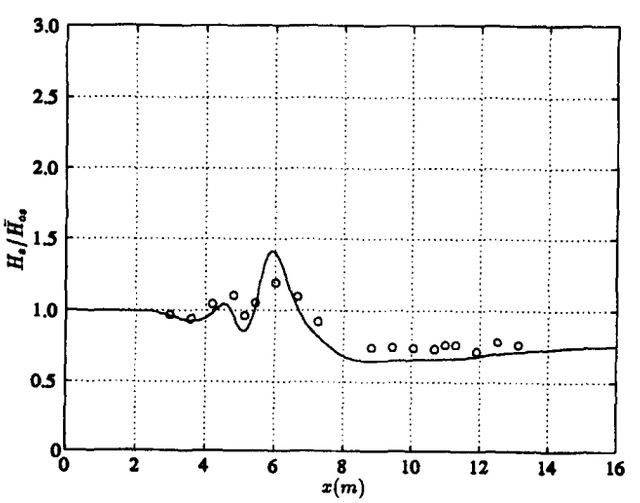

FIG. 12. Data-to-Model Comparisons of Significant Wave Heights along Transect A-A (Test 6: More Energy, Broad Directional Spread)

model tends to overpredict the wave height. This is probably because of the severe focusing seen in Fig. 7. Another probable cause for the discrepancy could be that the focusing is taking place in the surf zone, and a different breaking model might give more accurate results.

Comparisons along the six transverse transects are shown in Figs. 13–16. Again, the circles represent data, whereas the solid line presents the model predictions. In all cases, the model predicts large wave heights at the side walls. This is because the no-flux boundary condition at the side wall causes

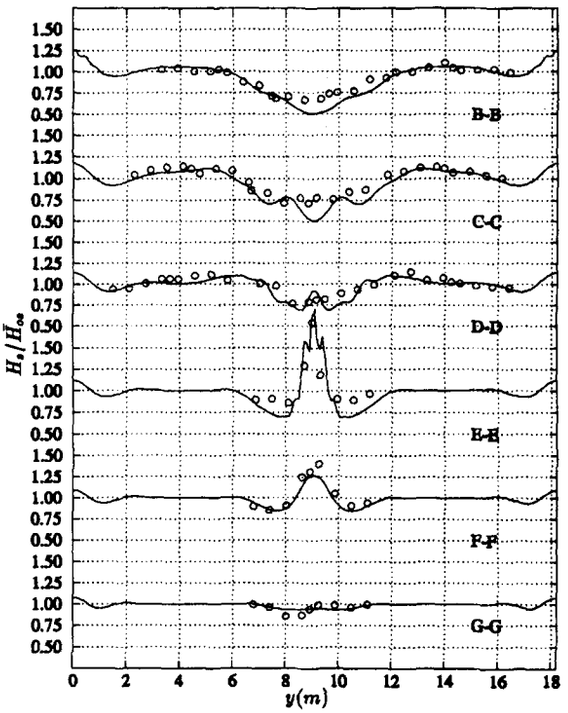

FIG. 13. Data-to-Model Comparisons of Significant Wave Heights for Test 3 (Less Energy, Narrow Directional Spread)

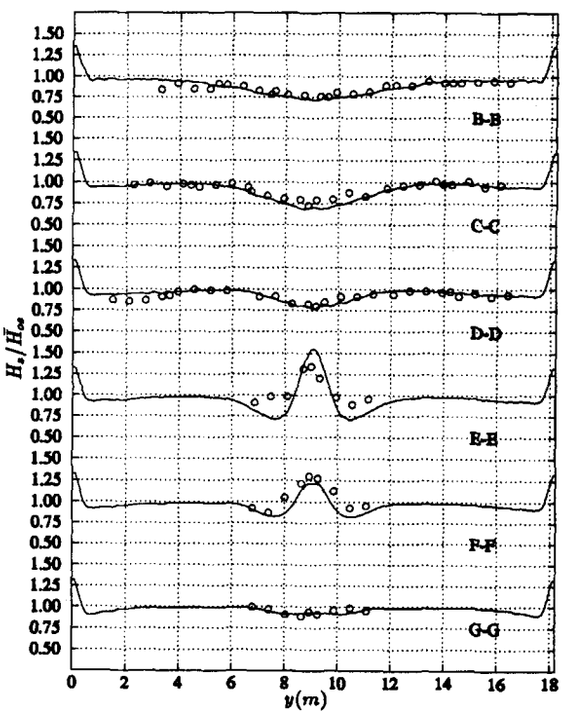

FIG. 14. Data-to-Model Comparisons of Significant Wave Heights for Test 4 (Less Energy, Broad Directional Spread)

the waves to form an antinode there, which when superimposed leads to large significant wave heights at the side walls. Along transect G-G, where the waves have not started to refract strongly, the model-to-data comparison is quite good. On top of the shoal (transect F-F), where the waves are focusing and breaking, this comparison is fair. The comparisons behind the shoal (transects E-E, D-D, C-C, and B-B), on the other hand, are extremely good.

An interesting observation in the model results is that, behind the shoal, spatial variations of the wave height are more

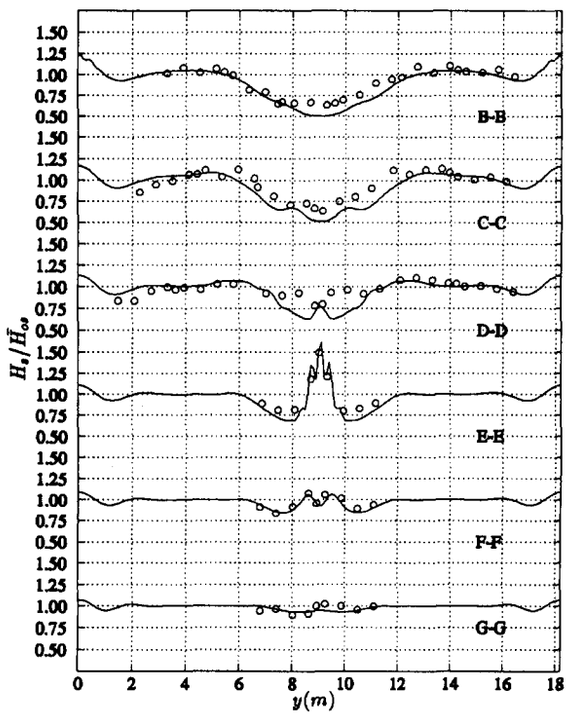

FIG. 15. Data-to-Model Comparisons of Significant Wave Heights for Test 3 (More Energy, Narrow Directional Spread)

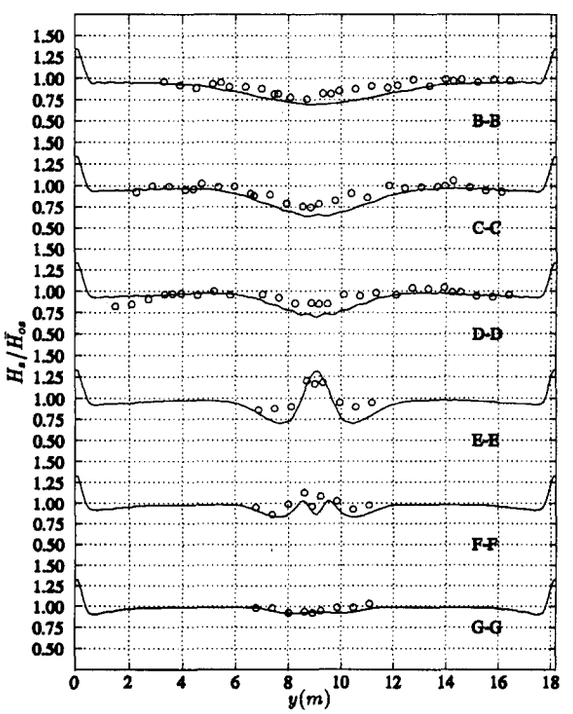

FIG. 16. Data-to-Model Comparisons of Significant Wave Heights for Test 6 (More Energy, Broad Directional Spread)

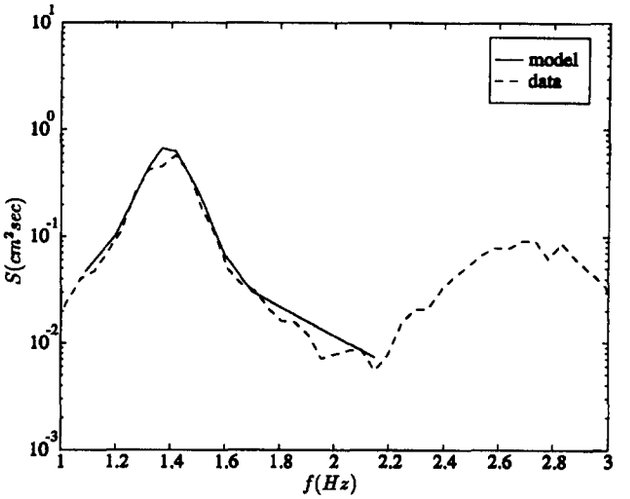

FIG. 17. Spectrum Comparison on Top of Shoal (Position 13, Gauge 5) for Test 3

a function of the type of directional distribution of the input spectrum, instead of being a function of the energy content of the spectrum. The wave height variation is more uniform for the broad directional spectrum tests (Tests 4 and 6) as compared to the narrow directional spectrum tests (Tests 3 and 5). Before the focusing takes place (transect F-F), the wave height variations for Tests 3 and 4 are quite similar, while the wave height variations for Tests 5 and 6 are quite similar, indicating that before the region of focus, the spatial variation of the wave height depends more on the energy content of the spectrum. This feature is also seen in the comparisons along transect A-A, where Tests 5 and 6 (Figs. 11 and 12) have a small peak in the wave height variation around $x = 5$ m (on top of the shoal) which is absent in Tests 3 and 4 (Figs. 9 and 10), whereas Tests 3 and 5 show a small peak around $x = 8$ m which is absent in Tests 4 and 6. Unfortunately, we cannot make the same conclusions by analyzing the data, because we do not have the resolution to make that observation clearly. The wave height variation behind the shoal is more smoothed out for a broad directional spread than for a narrow directional spread. A detailed explanation of this smoothing effect as a manifestation of cancellation (due to superposition) of details in the wave height pattern of each individual wave is given by Panchang et al. (1990).

Frequency Spectra

The model, being based on a linear superposition of monochromatic wave components, is unable to predict wave-wave interactions. These interactions lead to the growth of higher harmonics in nature, and become more pronounced with increased nonlinearity. A comparison of model spectra [calculated from (8)] with data spectra on top of the shoal (Fig. 17) shows this disparity quite clearly. The higher harmonics (second peak) in the data have a considerable amount of energy compared to the primary wave field (first peak), but are not predicted at all by the model. Such a growth in the energy of the higher harmonics is absent further downwave of the shoal (Fig. 18), and is seen in the data only on top of the shoal and in the region of focus where the wave field is highly nonlinear. This effect is probably partly responsible for the disparity in the significant wave height comparisons around and on top of the shoal.

Angle Distribution

Angle distributions can only be obtained for the model results because all the data was collected in the form of a time

series of the surface elevation, from which angle distributions can only be obtained if the wave field is homogeneous, which is not the case here. Even though no comparisons can be made between model and data results, a clear picture of the physics involved can be obtained.

For all four spectral tests, the directional spectrum initially has an average angle to the wavemaker ($\bar{\theta} = 0°$). Thus, the average angle should be 0° everywhere if the shoal is not present. Due to refraction effects from the shoal, the average angle deviates from 0°, as can be seen in Fig. 19, where the gauge locations are also indicated. The values of the average angles are given by the directions of the arrows. Fig. 19 gives us the predominant direction of the spectrum, and shows the same focusing effect that is seen in the refraction diagram of a monochromatic wave (Fig. 7). Due to severe focusing, the spectrum crosses from the left half of the basin to the right and vice versa. Wherever the spectra from the two sides cross each other the overall spectrum becomes very complicated. The symmetry of the bathymetry leads to a symmetry in the average angle distribution. Comparisons of Figs. 7 and 19 show that, though the random waves and monochromatic waves show similar trends in angular distributions, there are still significant differences between the two cases. Just as with wave height variations, it would be quite erroneous to approximate random waves by a representative monochromatic wave when trying to estimate the predominant direction of the spectrum at different locations. O'Reilly and Guza (1991) show how a directional spectrum evolves over a submerged shoal using a refraction model, which, however, does not account for diffraction effects or wave breaking.

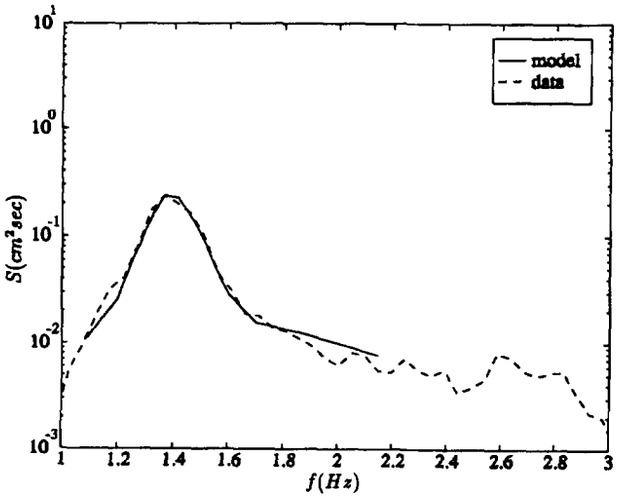

FIG. 18. Spectrum Comparison Downwave of Shoal (Position 4, Gauge 5) for Test 3

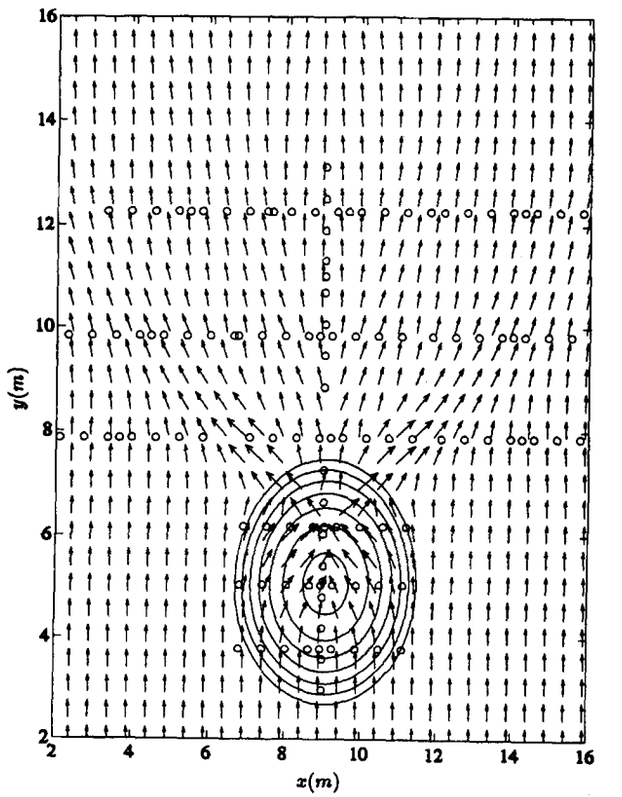

FIG. 19. Average Angle Distribution with Gauge Locations (○)

CONCLUSION AND SUGGESTIONS

A numerical model has been presented that simulates the evolution of wave spectra over a gently sloping bottom, in the presence of wave breaking. The model discretizes the directional spectrum into directional wave components and uses a monochromatic parabolic wave model to predict the evolution of these wave components independently. A statistical model is used to simulate dissipation due to wave breaking. For the one-dimensional case, the model predicts the shoaling and breaking characteristics of the waves quite well.

The model was also tested for waves breaking over a circular shoal and comparisons with experimental data gave good results. The wave height variation behind the shoal was more a function of the directional spread of the input wave condition, rather than a function of the energy content, with the variation being more smoothed out for the cases with broad directional spreading as compared with the cases with narrow directional spreading. The drawback of the model has been its inability to predict wave-wave interactions, which become important on top of the shoal where the waves are breaking and highly nonlinear. Studies of the frequency spectrum have shown the presence of secondary peaks formed due to these higher harmonics that are not reproduced by the model. Another limitation of the model is its parabolic nature, which limits its range of angles to ±45°. Due to this, some of the sharply focusing rays on top of the shoal cannot be reproduced by the model, which is probably the cause of the discrepancy between the data and the model results in this area. To get a better idea as to whether the discrepancy between the data and the model on top of the shoal is due to the limitations of the numerical model or to errors in the experimental data, comparisons need to be made with a model which will be able both to simulate waves with no limitations on the range of angles and to predict the generation of higher harmonics on top of the shoal.

The breaking model used in this numerical model was designed for one-dimensional breaking waves, and has not been modified to take into account directional effects. Also, the breaking model assumes that the waves after breaking do not reform. For the cases where waves reform after breaking (e.g., waves over a shoal), the dissipation is reduced. However, this reduction is probably introduced much faster than the rate at which it occurs in nature, and it remains to be seen whether the results on top of the shoal would improve using a different breaking model.

ACKNOWLEDGMENTS

This research has been sponsored by the U.S. Army Corps of Engineers, Coastal Engineering Research Center (Contract No. DACW 39-90-D-0006-D002) and by the NOAA Office of Sea Grant, Department of Commerce, under Grant No. NA/6RG0162-01 (Project No. R/OE-9).

APPENDIX. REFERENCES

Berkhoff, J. C. W. (1972). "Computation of combined refraction diffraction." *Proc., 13th Int. Conf. on Coast. Engrg.*, Vancouver, Canada, 471–490.

Booij, N. (1981). "Gravity waves on water with non-uniform depth and current." Communication on Hydraulics; *Rep. No. 81-1*, Department of Civil Engineering, Delft University of Technology, Delft, The Netherlands.

Borgman, L. E. (1984). "Directional spectrum estimation for the S_{xy} gages." *Tech. Rep.*, Coastal Engineering Research Center, Vicksburg, Miss.

Bouws, E., Gunther, H., Rosenthal, W., and Vincent, C. (1985). "Similarity of the wind wave spectrum in finite depth water." *J. Geophys. Res.*, 90, 975–986.

Chawla, A. (1995). "Wave transformation over a submerged shoal," MS thesis, University of Delaware, Newark, Del.

Goda, Y. (1985). *Random seas and design of maritime structures*. Univ. of Tokyo Press, Tokyo, Japan.

Grassa, J. M. (1990). "Directional random waves propagation on beaches." *Proc., 22nd Int. Conf. on Coastal Engrg.*, Delft, The Netherlands, 798–811.

Isobe, M. (1987). "A parabolic model for transformation of irregular waves due to refraction, diffraction and breaking." *Coast. Engrg. in Japan*, Tokyo, Japan, 30, 33–47.

Izumiya, T., and Horikawa, K. (1987). "On the transformation of directional waves under combined refraction and diffraction." *Coast. Engrg. in Japan*, Tokyo, Japan, 30, 49–65.

Kirby, J. T. (1984). "A note on linear surface wave-current interaction over slowly varying topography." *J. Geophys. Res.*, 89, 745–747.

Kirby, J. T. (1986a). "Higher-order approximations in the parabolic equation for water waves." *J. Geophys. Res.*, 91, 933–952.

Kirby, J. T. (1986b). "Rational approximations in the parabolic equation method for water waves." *Coast. Engrg.*, 10, 355–378.

Kirby, J. T., and Dalrymple, R. A. (1983). "A parabolic equation for combined refraction diffraction of Stokes waves by mildly varying topography." *J. Fluid Mech.*, Cambridge, U.K., 136, 453–466.

Kirby, J. T., and Dalrymple, R. A. (1984). "A verification of a parabolic equation for propagation of weakly nonlinear waves." *Coast. Engrg.*, 8, 219–221.

Kirby, J. T., and Kaihatu, J. M. (1996). "Structure of frequency domain models for random wave breaking." *Proc., 25th Int. Conf. on Coastal Engrg.*, Orlando, 1144–1155.

Lie, V., and Tørum, A. (1991). "Ocean waves over shoals." *Coast. Engrg.*, 15, 545–562.

Mase, H., and Kirby, J. T. (1992). "Modified frequency-domain KdV equation for random wave shoaling." *Proc., 23rd Int. Conf. on Coastal Engrg.*, Venice, 474–487.

O'Reilly, W. C., and Guza, R. T. (1991). "Comparison of spectral refraction and refraction-diffraction wave models." *J. Wtrwy., Port, Coast., and Oc. Engrg.*, ASCE, 117(3), 199–215.

Özkan, H. T. (1993). "Evolution of breaking directional spectral waves in the nearshore zone," MS thesis, University of Delaware, Newark, Del.

Özkan, H. T., and Kirby, J. T. (1993). "Evolution of breaking directional spectral waves in the nearshore zone." *Proc., 2nd Int. Symp. on Wave Measurement and Analysis*, New Orleans, 849–863.

Panchang, V. G., Wei, G., Pearce, B. R., and Briggs, M. J. (1990). "Numerical simulation of irregular wave propagation over shoal." *J. Wtrwy. Port, Coast., and Oc. Engrg.*, ASCE, 116(3), 324–340.

Radder, A. C. (1979). "On the parabolic equation method for water wave propagation." *J. Fluid Mech.*, Cambridge, U.K., 95, 159–176.

Thornton, E. B., and Guza, R. T. (1983). "Transformations of wave height distribution." *J. Geophys. Res.*, 88, 5925–5938.

Vincent, C. L., and Briggs, M. J. (1989). "Refraction-diffraction of irregular waves over a mound." *J. Wtrwy. Port, Coast., and Oc. Engrg.*, ASCE, 115(2), 269–284.